ALUMINIUM-RICH SILICA SCALING: SAN JACINTO-TIZATE GEOTHERMAL ENERGY PROJECT, NICARAGUA

Claire J Newton [1*], Sadiq J Zarrouk [1], Jim Lawless [2], Michael C Rowe [1], J A Guidos [3], Kevin L Brown [4]

[1] The University of Auckland, Private Bag 92019, Auckland, New Zealand

[2] Polaris Infrastructure Ltd, 77 Bloor Street West, Suite 600 Toronto, Ontario, Canada M5S 1M2

[3] Polaris Energy Nicaragua S.A. Km 114 Carretera León-Malpaisillo, León, Nicaragua

[4] Geokem, P.O. Box 30-125, Barrington, Christchurch 8244, New Zealand

*claire.newton@outlook.co.nz

Keywords: *San Jacinto-Tizate, Aluminium-rich, silica scale, reinjection line, XRD, FESEM EDS, allophane, hydroxyaluminosilicate, boehmite.*

ABSTRACT

Geothermal pipeline scale sampled from four locations along the San Jacinto North Reinjection Line was found to consist of metal-rich amorphous silica containing up to 16 wt. % Al_2O_3, 6.9 wt. % Fe_2O_3, 4.1 wt. % K_2O, and 2.7 wt. % Na_2O; with some zones of the scale significantly enriched with Au-Ag mineralised Cu-Fe-Zn-Pb sulfides. X-ray Diffraction (XRD) patterns and Field Emission Scanning Electron Microscope energy dispersive spectroscopy (FESEM EDS) in-situ compositional analyses confirm that Al, Na, K, Ca and some Fe are contained within the amorphous silica molecular structure, with remaining Fe as sulfide minerals and corrosion products. Al is the most abundant metallic element in all scale samples, with Na, K, and Ca concentrations closely correlating with Al. Fe is concentrated in the earliest formed scale yet is rare to absent in the most recently deposited scale, and is likely derived from corrosion of steel pipe and well casings. The concentration of Al in silica scale reduces with distance from the production well heads, and is most concentrated in the earliest deposited base of the scale, which contains 4-12 wt. % Al_2O_3 (bulk area analyses) and 10-16 wt. % Al_2O_3 (in-situ colloids). The most recently deposited silica contains ~11 wt. % Al_2O_3, both bulk zones and colloids. The contrast between bulk and in-situ metal concentrations reflects the observation (via FESEM) that the scale is largely an admixture of primary metal-rich silica colloids, and pure SiO_2 mantling this earlier deposited matrix. The broad XRD peaks are typical of amorphous silica yet they also show a systematic 2Θ angle shift positively correlated with aluminium concentration. These characteristics closely resemble those both of aluminium-rich silica scales from other geothermal fields, and hydroxyaluminosilicates (HAS) precipitated in lab experiments. A novel reaction pathway based on these observations, along with recent experimental and computational chemistry research into the formation of HAS, is proposed. This mechanism accounts for both the lack of apparent silica polymerisation induction period in cases of aluminium-rich silica scaling and its deposition in solutions undersaturated with respect to amorphous silica, observed both in scaling experiments and in the field at San Jacinto, and several other geothermal power stations worldwide.

1. INTRODUCTION

Aluminium-rich amorphous silica scales have been observed to form from brines in geothermal pipelines at a number of geothermal fields internationally (Table 1); often accumulating at higher rates and temperatures than would be expected for pure amorphous silica scales (Gallup, 1998; Raymond et al., 2005), including at San Jacinto-Tizate (Thermochem, 2010). Aluminium-rich silica scales have been observed in Iceland (Thorhallsson et al., 1975; Arnórsson, 1981) Japan, (Ichikuni, 1970; Yokoyama et al., 1989, Yokoyama et al., 1993; Yokoyama et al., 1999), the Philippines and Indonesia (Gallup, 1997), New Zealand (Reyes et al., 2001; Mroczek et al., 2000), El Salvador (Raymond et al., 2005), and at San Jacinto-Tizate, Nicaragua (Thermochem, 2010; this report). These scales lack significant clay phases yet contain up to approximately 10 w.t.% Al_2O_3, despite aluminium concentrations of only 0.2 to 1 ppm in the affected geothermal brines (Thorhallsson et al., 1975; Yokoyama et al., 1993; Gallup, 1997; Raymond et al., 2005). These usually hard, dense, and mechanically strong deposits can present significant problems for the utilisation of geothermal energy as they can rapidly block pipes and valves, and reduce the injection capacity (injectivity) of geothermal brine reinjection wells. These effects result in costly equipment shutdowns for well and pipeline maintenance work, as well as reducing geothermal electricity output from the power-plant.

Electricity production at San Jacinto-Tizate began in 2005 with the commissioning of two 5 MWe back pressure turbines (Units 1 and 2); with anomalous, sub silica-saturation, aluminous-silica scaling observed at as early as 2010 in the SJ1-1 brine injection well head, and decommissioned SJ6-1 reinjection line (Thermochem, 2010). In 2012, two 36 MWe condensing turbines (Units 3 and 4) were commissioned, which utilise steam from several recently developed high enthalpy geothermal wells. Two of these wells, SJ12-2 and SJ12-3 produce fluid (1280 and 1370 kJ/kg respectively) with a silica concentration of approximately 700 ppm (total discharge), the highest concentrations reported at San Jacinto (Libbey et al., 2017). Brine from these wells is discharged via a steam separator (HPS3) into the North Reinjection Line (NRL), and subsequently reinjection well SJ-11-1. Since being put into use in 2012, the NRL has experienced rapid silica scaling, which was been accompanied by significant injectivity decline in SJ11-1 (Escobar and Escalante, 2015; Libbey et al., 2017). In an attempt to combat this scaling, dosing of the geothermal brine with a series of commercial silica dispersant/anti-scalant products was trialled from mid-2014 through to mid-2016, with none of these agents proving to be fully effective (Escobar and Escalante, 2015). Following this, two organic acids were trialled beginning in November 2016; with both acetic and citric acid proving effective at controlling silica polymerisation of brine in the NRL (Matus and Guidos, 2017), with acetic acid being finally

Table 1. Instances of aluminium-rich scale reported in the literature compared to host reservoir characteristics.

Citations: *Awibengkok*; Gallup, 1997; Stimac at al., 2008. *Silangkitang*; Gallup, 1997. Hickman et al., 2004. *Bulalo*; Gallup, 1997; Clemente and Villadolid-Abrigo, 1993. *Ohtake*; Yokoyama et al., 1993; Fujino and Yamasaki, 1985. *Hatchobaru*; Yokoyama et al., 1993; Fujino and Yamasaki, 1985. *Takigami*; Yokoyama et al., 1993; Takenaka and Furuya, 1991. *Makizono (Ogiri*); Yokoyama et al., 1993; Itoi et al., 2010; *Rotokawa*; Reyes et al., 2003; McNamara et al., 2016. *Berlin*; Raymond et al., 2005; Portier et al., 2010. *San Jacinto*; Libbey et al., 2017; White et al., 2008.

Location	Scale Al_2O_3 w.t.%	Brine Al ppm	pH	Well T_{max} ^oC	Dominant reservior host rock	Reservoir permeability
Awibengkok	10.00	0.1-1.0	6.8	312	Andesite-basltic andesite	Fracture controlled
Silangkitang	9.30	0.1-1.0	8.5	320	Metseds, silic tuffs, andesite	Fracture controlled
Bulalo	7.50	0.1-1.0	6.5	330	Andesite	Fracture controlled
Ohtake	7.95	0.28	8.3	*NS*	Hbl-Px andesite/deep felsic	Fracture controlled
Hatchobaru	4.57	0.69	7.9	*NS*	Hbl-Px andesite/deep felsic	Fracture controlled
Takigami	10.00	0.60	9.1	250	andesite, dacite-andesite	Fracture controlled
Makizono (Ogiri)	7.87	1.34	8.5	232	Hbl-Px andesite & metased	Fracture controlled
Rotokawa	7.04	*NS*	*NS*	330-340	Andesite, greywacke	Fracture controlled
Berlin (El Salvador)	8.90	0.1-1.9	6.7	290	Basaltic andeseite	Fracture controlled
San Jacinto	6.17	0.36	7.0	300	Basalt, basaltic andesite	Fracture controlled

selected for longer term testing in March 2017.

During maintenance work in early 2017, samples of scale from four locations on the San Jacinto-Tizate NRL were collected by Polaris Energy Nicaragua S.A. (PENSA) staff and sent to New Zealand for analysis. The aims of this study were to characterize deposit's compositional variation with distance along the NRL (via X-ray Fluorescence (XRF)), its chemical and microstructural variation with time at each location within the NRL (via Field Emission Scanning Electron Microscope (FESEM)), and its mineralogy and crystal structure (via X-ray diffraction (XRD)). These data were then compared to that collected from similar metal-rich silica scales which occur at several other geothermal fields internationally. Finally, this enlarged compositional and structural dataset was then compared to that produced as a result of relatively recent work investigating hydroxyaluminosilicates (HAS) (Exley and Birchall, 1993; Tokoro et al., 2014; Leiviskä et al., 2014; Beardmore et al., 2016), which may yield insight into a potential formation mechanism of these deposits.

2. MATERIALS AND METHODS

Scale Samples were collected from four locations in the NRL by PENSA site personal in January and February 2017 during routine cleaning, monitoring, and maintenance work. The 'Reinjection Line-1' (RL1) sample was collected from the NRL, approximately 150 metres downstream of the outlet of HPS3. Sample RL2 was collected approximately 350 metres downstream of HPS3, and 40 metres north of a junction point between the NRL and the Southern Reinjection Line (excess brine from HPS3 was being directed to SJ1-1 and SJ10-1 reinjection wells in the south of the field). RL3 was collected 200 metres to the south of the Northern-Southern Reinjection Line Junction, and RL4 was collected from the SJ11-1 wellhead filter basket (scale was formed in-place) approximately 2 km downstream from HPS3.

Representative portions of each sample (approximately 100 grams of each) were crushed with a Boyd Crusher to produce up to 5mm diameter fragments. Both RL1 and RL2 crushed samples were each divided in half, with dark and light coloured fragments manually picked and separated from one of the halves of each divided bulk sample. These picked dark and light coloured samples were labelled RL1b/RL2b and RL1c/RL2c, respectively; with the unpicked, portions labelled RL1a/RL2a. Samples RL3 and RL4, although not completely homogeneous, had only subtle variations in colour and morphology, and are much thinner in cross-section compared to RL1 and RL2; making manual picking and colour separation impractical. All samples were then dried at 80^{o}C for 36 hours before being crushed to a fine powder with a Rocklabs tungsten ring mill. Scale composition was determined using a PANalytical Axios 1kW wavelength dispersive X-ray fluorescence (XRF) spectrometer, and mineralogy and crystallinity of the scale was obtained using a PANalytical Empyrean X-ray diffractometer (XRD). Representative intact scale clasts from each sampling location, which preserved complete cross-sections of the scale perpendicular to the geothermal brine flow, were selected. These clasts were fractured in a Rocklabs hydraulic rock splitter to obtain fresh, flat, intact faces. In-situ micro-chemical analyses and imaging of these were conducted with a Philips XL30S Field Emission Gun Scanning Electron Microscope (FESEM), equipped with a Si-Li (Lithium drifted) Energy Dispersive Spectrometer (EDS). The instrument was operated in backscatter mode, which results in higher atomic mass elements appearing brighter; this has the benefit of highlighting metal sulfides, metal oxides, and any iron-rich clay minerals etc. A total of 80 in-situ micro-chemical spot analyses were carried out along transects of the prepared and sputter coated RL1, RL2 and RL4 scale faces in the direction of scale growth. The primary intent of the micro-chemical transects was to characterise and record any changes in the composition and morphology of the silica within each sample, and between samples. The composition of accompanying sulfide minerals was also determined, along with any rare clay or other minerals.

3. RESULTS AND DISCUSSION

3.1 General characteristics

In general, the colour intensity, metal content, and thickness of the silica scale collected from the NRL all reduce with distance from HPS3. Additionally, as can be seen from Fig. 1, the appearance of the scale at each sampling location is also highly variable in cross-section. The bulk compositions of the NRL scale samples and that of their colour-picked derivatives, as revealed via XRF (Table 2), indicate that colour (Fig. 1 and Table 1) is indicative of composition. This was also observed by Yokoyama et al. (1993) who investigated very similar metalliferous silica scales which

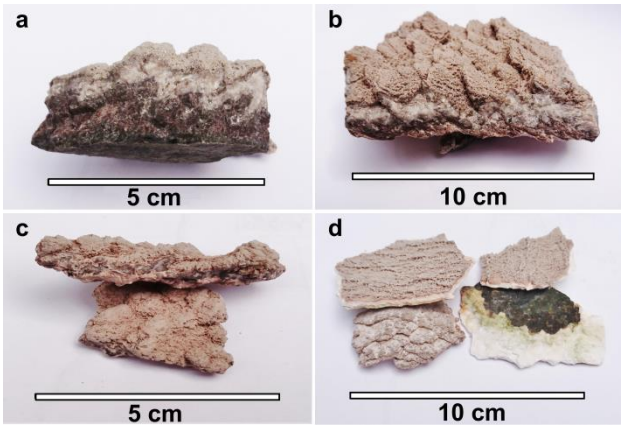

Fig. 1. Representative scale clasts of scale from the San Jacinto-Tizate's North Reinjection Line, a; RL1, b; RL2, c; RL3, d; RL4, the dark material attached to the lower-right RL4 scale clast is surface corrosion from the filter-basket inner pipe-wall.

occur at several geothermal fields in Japan. The base of RL1 (RL1b) has the greatest iron content, and displays colours ranging from dark reddish brown to almost black. The slightly translucent white-grey to light brown coloured silica of the top section of RL1 (RL1c), which also makes up much of RL2, is indicative of moderate to relatively high aluminium but low iron concentration; while the opaque white silica, which comprises most of the volume of RL4 is almost pure SiO_2. The brown layer visible on the top, fluid facing, surfaces of all samples represents a sudden increase in the aluminium content (resolved via SEM-EDS micro-chemical analyses) in the scale most recently deposited along the entire length of the NRL; which is possibly related to recent acid dosing. Distinct flow textures are also evident in the scale, which appear as chevron patterns in cross-section, and take the form of flat triangular to semi-circular blades, or sharp curvilinear ridges orientated perpendicular to brine flow direction in three dimensions. Both the blades and ridges form with their sharp edge facing the direction of flow, and appear to grow via colloids impacting and accumulating on this leading edge. This largely rules out conductive cooling of stationary brine during pipeline shut-down events as a significant source of pipeline scale accumulation.

3.2 Scale composition in detail

Also revealed by the bulk XRF chemical analyses (Table 2) is the correlation of alkali element concentration to the scale's aluminium content; this was also noted by previous workers such as a Yokoyama (1987, 1993, and 1999), and Gallup (1997 and 1998). These investigators attributed this to the replacement of Si^{4+} with Al^{3+} in the scale lattice, resulting in a charge imbalance, which is then compensated for by the introduction of interstitial ions such as sodium, potassium and calcium. Micro chemical in-situ analyses via SEM-EDS confirm that the alkali elements and aluminium (and some Fe) are in fact contained within the molecular structure of the amorphous silica in these samples, with the only aluminosilicate minerals encountered being rare fragments of epidote transported from the reservoir. Freshly deposited silica spheroids at the top of the scale samples were found to also contain high Al, K and Na, indicating that alkali element uptake is rapid, and likely occurs during initial colloid formation and growth. When viewed at high

Table 2. Major element XRF analyses of San Jacinto North Reinjection Line scale (w.t.%).

Sample	SiO_2 %	Al_2O_3 %	K_2O %	Na_2O %	Fe_2O_3 %	CaO %
RL1a	81.5	6.2	1.77	1.42	1.33	1.06
RL1b	82.3	6.1	1.69	1.36	1.67	1.04
RL1c	86.8	6.3	1.95	1.62	0.53	0.95
RL2a	87.4	4.1	1.27	1.10	0.34	0.59
RL2b	84.1	5.2	1.48	1.20	0.58	0.80
RL2c	88.3	3.4	1.11	0.98	0.16	0.44
RL3	88.0	3.7	0.97	0.89	0.43	0.51
RL4	96.9	0.2	0.07	0.13	0.03	0.09

magnification via SEM, it becomes apparent that the metal content of the silica not only affects its colour, but also its texture (Fig. 2). The scale containing the greatest metal concentrations (especially iron) often appears to have a rough, uneven/mottled appearance (Fig. 2a.), which may be due to rapid scale precipitation and agglomeration. These rough textured, high metal (especially iron) content scale zones typically also contain abundant sulfide minerals; mostly pyrite and chalcopyrite, often with Zn and Pb, which are also frequently Ag-Au mineralized. These rough textured zones of iron (and aluminium) rich silica and abundant iron bearing sulfides mostly occur in the lower several millimeters of RL1 and RL2 scale samples. This is suggestive that oxidation, and dissolution reactions involving the then relatively new mild steel well liners and surface pipes may have contributed to deposition of this variety of scale. In contrast to iron, which is only present in relatively low concentration in the most recently deposited scale, aluminium continues to be concentrated in, and likely contributes to, silica scaling within the NRL. Several SEM-EDS analyses from the topmost, latest deposited, silica in both RL1 and RL2 indicate a recent reappearance of relatively significant Fe (1.1-1.3 w.t. % Fe_2O_3), however, which may be indicative of corrosion bought about by recent acid dosing of NRL brine; which may also account for the brown tint visible in in the top layer of all NRL samples.

Smooth, merged, globular textured silica contains very little to no Al (0-2 w.t. % Al_2O_3 as resolved via SEM-EDS), while the smaller and irregularly shaped metal-rich silica spheroids contain between 10 and 16 w.t. % Al_2O_3 (fig. 2.), up to 6.9 wt. % Fe_2O_3, and typically 2-4 wt. % K_2O, ~2 wt. % Na_2O and ~1 w.t. % CaO. Smooth, merged low-Al silica appears to be mantling earlier deposited metal-rich silica (fig. 2a), sometimes completely filling the void spaces within the initially quite open metal-rich silica scale structure. It is likely that this smooth merged silica is in fact composed of pure SiO_2, with SEM-EDS analyses of smooth silica sometimes capturing some of the neighboring high-Al silica zones. Additionally, no identifiable primary silica colloids of intermediate composition between >0 and <10 w.t.% Al_2O_3 were observed. The concentration of Al in silica scale reduces with distance from the production well heads, and is also most concentrated in the earliest deposited base of the scale, with 4-12 wt. % Al_2O_3 in the bulk scale (in-situ colloids up to 16 wt. % Al_2O_3). This is followed by a decrease in Al_2O_3 concentration to 3-10 wt. % in the mid-section of the bulk scale (10-14 wt. % Al_2O_3 in-situ) for the two upstream-most samples, which is then followed by a marked increase in metal content to ~11 wt. % Al_2O_3 (both bulk and in-situ) in in the most recently

deposited scale. High-Al (+K, Na, and Ca) silica spheroids are visible in top sections of all three samples analysed via SEM-EDS. These appear to represent the earliest generation of silica deposited from the fluid, with these colloids forming the initial building blocks of silica scale depositing in the NRL at San Jacinto-Tizate. The deposition and agglomeration of these first spheroids is then likely followed by further reaction with, and precipitation of, monomeric silica directly from solution, which further 'cements' and increases the volume of the scale. Smooth, globular low Al/pure SiO2 silica is only observed in small void spaces within the primary scale matrix. These spaces will have been only very indirectly in communication with, if at all, the main brine flow within the line. It seems likely that these low Al/pure SiO2 silica 'spheres' are the product of silica precipitation from conductively cooling Al-depleted brine which has been trapped by scale growth, or which has penetrated deep into the scale matrix

3.3 Scale mineralogy/crystallinity

Aside from small quartz peaks, the XRD patterns (Fig. 3) produced by the NRL samples are dominated by broad XRD peaks typical of amorphous opaline silica. The more intense quartz peaks of RL1b and RL2b, compared to their un-picked bulk equivalents (RL1a and RL2a), are likely due to more a more advanced state of silica diagenesis in the separated darker (basal) material, reflective of the comparatively greater period of time elapsed since deposition of this silica. This phenomenon was also noted by Reyes et al. (2001) who investigated similar metalliferous scales deposited by brines from a high enthalpy andesite hosted reservoir at Rotokawa, New Zealand; and is likely analogous to the natural process of silica diagenesis (e.g. Williams and Crerar 1985). While the broad XRD peaks of each sample are fairly similar in appearance, they do show a systematic compositionally dependent 2Θ shift as the aluminium content in the scale varies; with greater Al concentration correlating with greater 2Θ angle (Fig. 3). A very similar trend was noted by Gallup (1998) and Tokoro et al. (2014). The broad peaks of the XRD patterns, together with the compositional dependence of the peak positions, indicates that the scale is almost exclusively composed of amorphous material, with Al, K, Na, Ca, and Fe substituting into the amorphous silica structure. These observations, combined with trend that of the greatest metal concentrations occurring in the upstream-most samples, closest to HPS3; both in the bulk scale, and the earliest deposited precipitate, is indicative that Al reacts with silica at a very early stage of silica scaling process. One of two possibilities may account for this, either aluminium is rapidly adsorbed by early polymerised silica; or that some rapidly polymerising/precipitating aluminium phase is reacting with monomeric silica in solution. A case for the latter reaction, informed by recent developments in hydroxyaluminosilicate research is discussed in the following section.

4. A POSSIBLIBLE SCALING-REACTION MECHANISM

The physical-chemical process responsible for the formation of aluminium-rich silica scales from the brines of some geothermal reservoirs, and not others, has remained elusive; with both aluminous and non-aluminous silica scales forming from geothermal brines of apparently similar chemical compositions (Arnórsson, 1981; Yokoyama et al., 1993; Arnórsson, 1995; Gallup 1997; Raymond et al., 2005). Both aluminous and non-aluminous silica scales

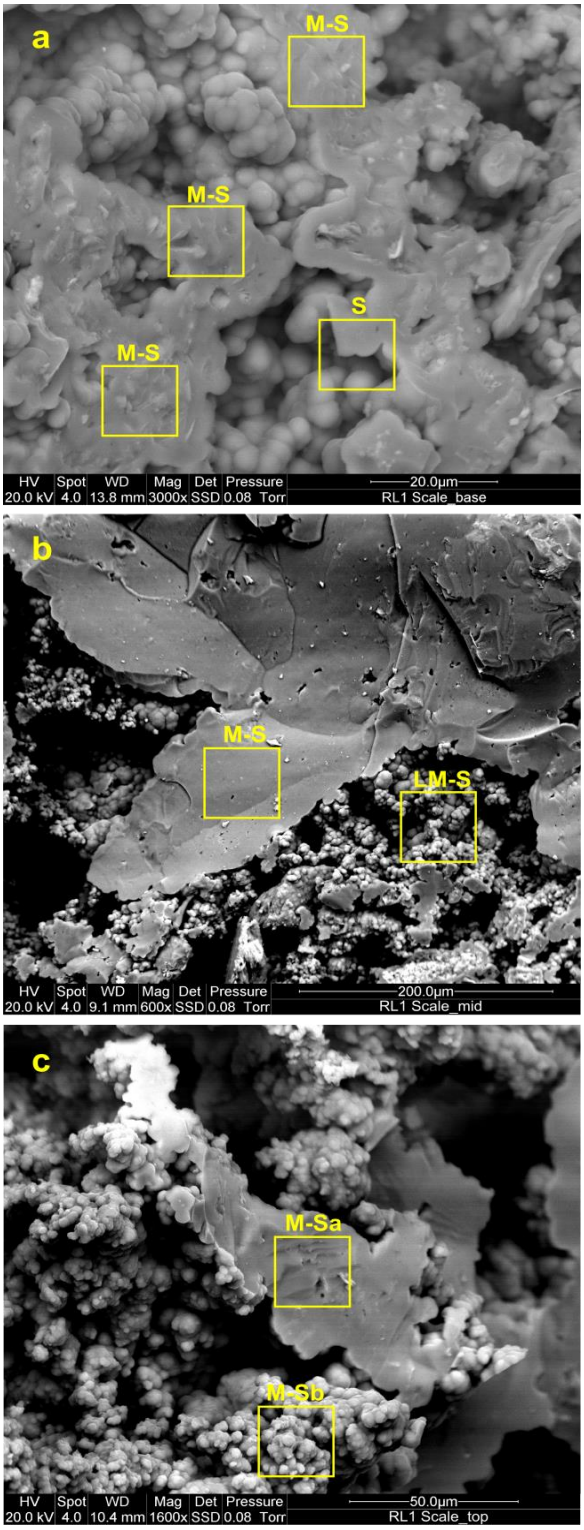

Fig 2. SEM images of San Jacinto-Tizate scale (RL1). a; near the base of RL1, rough textured Al_2O_3 15 w.t.%, Fe_2O_3 3-4 w.t.% metalliferous silica (M-S), mantled with pure SiO2 (S). b; near middle of scale section, vitreous 6.5 w.t.% Al_2O_3 (M-S) silica, and globular, lower metal concentration silica (LM-S) containing 2 w.t.% Al_2O_3. c; view of the top of RL1, coalesced recently deposited metalliferous silica (M-Sa) containing 12 w.t.% Al_2O_3, and very recently deposited metalliferous silica spheroids (M-Sb) containing 10 w.t.% Al_2O_3.

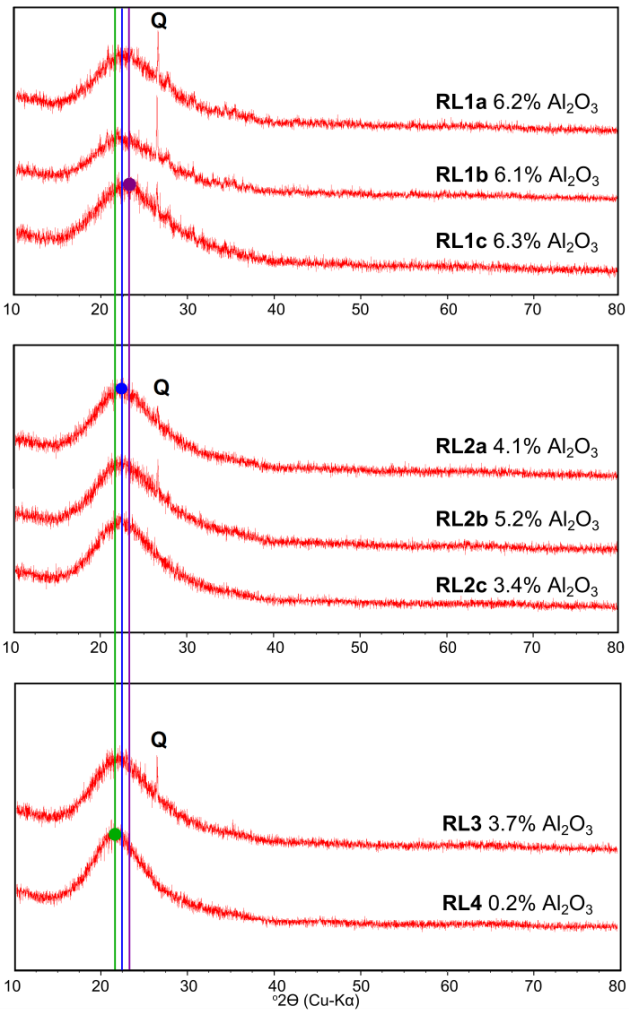

Fig 3. XRD patterns of San Jacinto NRL scale. Quartz peaks (Q) are visible in RL1, RL2, and RL3 at 26.6º. Coloured vertical lines have been added to illustrate changes in peak positions. The purple line highlights the RL1c peak at 23.3º, the green line indicates the RL4 peak centred at 22º (equal to that of cristobalite), while the blue line passes through the centre of the RL2a peak at approximately 22.7º 2Θ.

form from solutions of similar temperature, over common ranges of near-neutral pH, salinity, monomeric silica, and apparent aqueous aluminium concentration; which typically ranges from 0.2 to 1ppm when measured at surface conditions (Yokoyama et al., 1993; Gallup, 1997). Clues as to why aluminium-rich silica scale may form from some geothermal brines and not others includes its very short-nil polymerisation induction period, as seen at San Jacinto, its formation at higher temperature than would otherwise be suggested by SSI calculations (Gallup, 1998; Raymond et al., 2005; Thermochem, 2010), and differences in reservoir geology between those geothermal fields which are, and which are not affected. Specifically, from instances of aluminium-rich silica scaling reported in the literature, it appears that it more commonly occurs where geothermal reservoirs are hosted in andesitic and basaltic rocks, rather than more silicic reservoir host rocks.

An intriguing reaction mechanism, proposed by Exley and Birchall (1993) to explain the formation of amorphous colloids composed of silica and aluminium, commonly referred to as hydroxy-aluminosilicates (HAS) in the biochemical, inorganic and industrial chemistry literature; may offer insight into the formation of geothermal aluminium-rich silica scale. This HAS reaction mechanism has since been thoroughly corroborated by numerous studies (e.g. Exley and Birchall, 1993; Doucet et al., 2001a; Doucet et al., 2001b; Strekopytov et al., 2006; Exley, 2012; Tokoro et al., 2014; Leiviska et al., 2014; Beardmore et al., 2016), with Al and Si-rich end member products designated HAS_A and HAS_B, respectively. These materials have close natural analogues, identified as protoimogolite and allophane, respectively, in the geoscience realm (Doucet et al. 2001b; Exley, 2012). The trigger mechanism for the production of HAS (and likely their natural analogues) is the supersaturation of aluminium, with respect to gibbsite [$Al(OH)_{3(S)}$], and will proceed in both silica-undersaturated and saturated solutions. The condensation of $Al(OH)_{3(S)}$ from an Al-supersaturated solution is followed by the competitive addition of monomeric silica across this molecular frame. This second step inhibits of the autocondensation of a pure $Al(OH)_3$ solid phase, and instead results in the rapid formation of highly insoluble amorphous HAS colloids of variable Al:Si stoichiometry (Exley and Birchall, 1993). To reiterate, as originally found by Exley and Birchall (1993), and since verified by a large number of later investigators (e.g. Doucet et al. 2001a; Tokoro et al. 2014; Leiviska et al., 2014; Beardmore et al., 2016), the triggering of this reaction relies on the supersaturation of aqueous aluminium only, and will proceed in the presence of monomeric silica regardless of its concentration in solution.

A likely natural example of the HAS reaction mechanism is the precipitation of amorphous materials very similar to protoimogolite and allophane from cold spring water at Silica Rapids on the flanks of the dormant Mt Ruapehu andesitic stratovolcano (Wells and Childs, 1977; Childs et al., 1990; Brigatti et al., 2013). The vigorously bubbling spring is approximately 7ºC with a pH of 5 (as measured in April 2018) at its outlet, with pH rising rapidly to neutral within several hundred metres downstream, likely due to exsolution of dissolved CO_2 gas. Approximately 80m downstream from the spring outlet, a cream coloured precipitate appears, coating the stream bed and its edges. This material is an amorphous hydroxyaluminosilicate of Si/Al mole ratio between 0.5 and 1, equivalent to HAS_A/protoimogolite and HAS_B/allophane, respectively. The spring water contains approximately 0.1 ppm Al at its outlet, which corresponds to saturation with respect to gibbsite at a pH of 4.8 [calculated via gibbsite solubility product constants of Wesolowski and Palmer (1994)]. At a pH of 5 (spring outlet) this solution becomes oversaturated with respect to gibbsite by a factor of 4, and by a factor of approximately 4000 as the water approaches neutral pH, several hundred metres downstream. In contrast, the spring water remains undersaturated with respect to amorphous silica, with a silica concentration approximately 30 ppm; which corresponds to a SSI of approximately 0.4 (Fleming and Crerar, 1982). It is therefore likely that the HAS reaction mechanism is also responsible for the deposition of this material.

Whether the HAS reaction mechanism operates at higher temperature and silica concentrations is still a moot point,

however. The experiments on which the HAS work is based were all carried out at room temperature and at relatively high aqueous Al:Si mole ratios, while monomeric silica concentrations ranged from zero to approximately 20% greater than saturation concentration for temperature (Exley and Birchall, 1993; Doucet et al. 2001a; Doucet et al. 2001b; Strekopytov et al., 2006; Tokoro et al. 2014; Leiviska et al., 2014). In all but a few of these experiments, the aluminium hydroxide saturation curve was approached from low pH, with Al^{3+} as the dominant aqueous Al species (see fig. 4). Whereas geothermal fluids used for electricity generation will (somewhat counterintuitively) almost exclusively intersect the boehmite/gibbsite solubility curve from its high-pH side, as this curve migrates toward higher pH as brine temperature reduces (Fig. 4), with $Al(OH)_4^-$ being the dominant aqueous Al species in these waters (Fig. 4). Despite these limitations, the results from these experiments do appear to be encouraging with regard to the possible validity of this mechanism at higher temperatures and silica concentrations. Within the range of silica concentrations studied, the rate of reaction increased with silica concentration (Exley and Birchall, 1993). Additionally, HAS-like materials are also reported to form from solutions approaching the aluminium hydroxide solubility curve from high pH, with some of these materials achieving much higher silicon concentrations than stoichiometric HAS_A and HAS_B (Exley and Birchall, 1993; Tokoro et al. 2014).

Some excellent feldspar dissolution-secondary mineral precipitation experimental studies conducted at geothermal temperatures (200-300ºC) by Murakami et al (1998) (anorthite) and Zhu and Lu (2009) (alkali feldspar) also offer valuable insight into hydrothermal reactions involving aqueous silica and aluminium. These studies found feldspar dissolution to be both rapid and incongruent. Overall, aluminium was found to dissolve most rapidly into product solutions, which quickly became supersaturated with respect to boehmite [(AlO(OH), the stable Al-oxyhydroxide mineral above 80ºC (Wefers and Misra, 1987; Moller et al., 2006; Palmer et al., 1996)]. In all experiments, boehmite was the first secondary-mineral product, appearing within hours in the Murakami et al. (1998) experiments. Solid boehmite then acts a sink for aqueous silica, slowly forming a poorly crystalline Al-silicate material referred to as 'modified boehmite' in the Murakami et al (1998), and Zhu and Lu (2009) works. Conversely, no quartz or amorphous silica was detected in the precipitation products in any of these experiments. Product solution chemistries rapidly evolved away from initial boehmite mineral stability into stability fields of clay minerals. Typically, product solution chemistry usually first crossed into the kaolinite field (though this was missed during some experiments), before finally entering the muscovite stability field, with solutions remaining supersaturated with respect to all three minerals. Somewhat surprisingly, boehmite (and modified boehmite) was found to be stable even when solution chemistry had evolved well outside of its stability field. In all experiments the dominant secondary mineral products were boehmite and 'modified boehmite', with some experiments producing detectible kaolinite after several hundreds of hours (others not at all), and none producing muscovite (above trace levels). Most significantly, these experiments demonstrate that the assumption of partial equilibrium between the fluid composition and secondary mineral products is not held under geologically brief time periods (on the scale of months to possibly a few years). Indicating instead, that

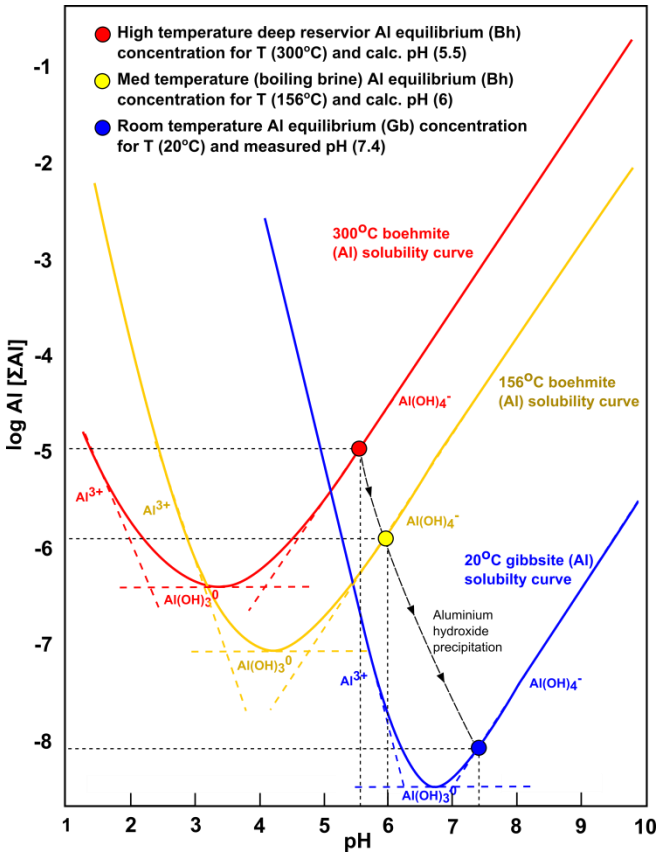

Fig. 4. Cartoon illustrating the effect of temperature and pH on aluminium (boehmite) solubility at conditions of the San Jacinto reservoir (red); boiling brine in HPS3 (yellow) [both pH values calculated via PHREEQC using data from Libbey et al. (2017)]; and at room temperature and pressure (blue) [surface measured pH from Libbey et al., 2017)]. Solubility curves were calculated using gibbsite and boehmite solubility products of Wesolowski and Palmer (1994), and Bénezeth et al. (2001), respectively.

though primary aluminosilicate mineral dissolution is initially fast, hydrothermal clay precipitation is in fact a slow kinetic process; with boehmite, and subsequently 'modified' boehmite likely acting as metastable steps during secondary hydrothermal aluminosilicate mineral alteration.

The solution experiments of Murakami et al (1998) Zhu and Lu (2009) were carried out under isothermal conditions, which is in stark contrast to the significant and rapid temperature changes experienced by geothermal fluids as they are extracted from the reservoir and finally travel through surface pipes. For fluids initially in thermal and chemical equilibrium with a geothermal reservoir, these thermal shocks are accompanied by, and are responsible for an equally rapid states chemical disequilibrium. This is somewhat more analogous to the instantaneous super saturation of Al with respect to gibbsite induced by pH adjustment during HAS experiments than the isothermal conditions of the feldspar dissolution-secondary mineral precipitation of Murakami et al (1998) Zhu and Lu (2009). A common example is the sudden super saturation of silica,

with respect to amorphous silica, due to steam flashing, which is responsible for pure amorphous-silica scaling. By comparison, the solubility of aluminium with respect to its stable aluminium oxy/hydroxide phase is far more temperature sensitive. To illustrate, the solubility of silica, with respect to amorphous silica, reduces by approximately a factor of 4 at neutral pH between 300ºC and 100ºC (Fleming and Crerar, 1982). In contrast, over this same temperature range and pH, the solubility of aluminium, with respect to boehmite, reduces by a factor of almost 90 [2.3 ppm @ 300ºC and 0.027 ppm @ 100ºC (Bénezeth et al., 2001)]. These calculated absolute Al oxyhydroxide saturation concentrations encompass those measured in almost all natural geothermal brines (e.g. Yokoyama et al., 1993; Gallup, 1997; Raymond 2005). However, in the case of aluminium (with respect to gibbsite/boehmite), solubility is also extremely pH dependent. In a boiling geothermal brine, CO_2 exsolution will simultaneously cause pH to increase as the brine temperature decreases; effects which in the case of a geothermal brine above pH ~ 4, act in opposition with regards to aluminium oxy/hydroxide solubility. A consequence of this is that the relative solubilities of gibbsite/boehmite on each side of a boiling event are highly dependent on initial solution composition and the details of the process. This may partially explain the somewhat random-seeming occurrence of aluminium-rich silica scaling.

Meanwhile, the trend of andesite-hosted reservoirs seeming to more commonly produce aluminium-rich silica scale may be explained by combining the above observations with the kinetic mechanism identified in the studies of Murakami et al (1998) Zhu and Lu (2009). The permeability of andesite hosted geothermal reservoirs is dominantly fracture controlled due to the high competency and low porosity of typical andesite lavas. Rapid fluid migration through discrete fracture systems may allow fluid from hot, precipitation limited active alteration zones to migrate rapidly towards production wells with little opportunity for chemical re-equilibration or interaction with reservoir host rock. It is proposed that some geothermal fluids, which are more likely to be encountered in andesite rock hosted reservoirs, may be enriched with aluminium in comparison to slower moving fluids in greater communication with reservoir host rocks, as is more usually the case in more porous, silicic rock hosted reservoirs.
This has yet to be tested however, as to date there have been no deep down-well measurements of geothermal aqueous aluminium concentrations (K. Brown, Pers. Comm. 2017).

Finally, these Al-enriched fluids may in some instances intersect the boehmite saturation curve during decompression induced boiling within or adjacent to geothermal production wells or steam separators, triggering a HAS style reaction, and resulting in the rapid precipitation of aluminium-rich silica colloids. Previously, adsorption of aqueous aluminium by silica polymers has been commonly invoked, as both the mechanism of aluminium uptake by silica, and the cause of aluminium-rich silica scaling (e.g. Yokoyama et al., 1989; Gallup, 1997; Gallup, 1998). However, this cannot explain aluminium-rich silica scaling which occurs below silica saturation, with respect to amorphous silica, as this requires silica to be already polymerised. Additionally, a novel experiment conducted by Bai et al. (2012) investigating the interaction of silica with aluminium adsorbed on Chelex resin at 25ºC and pH 8 found that aluminium ions at did not interact with polymerized silica. Conversely, monomeric silica rapidly adsorbed to Al-Chelex resin in solutions both undersaturated and supersaturated with respect to amorphous silica. Interestingly, these silica adsorption sites then acted as a template for the successive adsorption of monomeric silica to form silica sheets around Al-Chelex particles, similar to the results of aluminium-silica co-precipitation experiments by Tokoro et al. (2014); a process which may also be important in the formation geothermal aluminium rich silica scales.

5. CONCLUSION

Metals, particularly aluminium, are concentrated into silica scale formed in the North Reinjection Line at San Jacinto-Tizate, which consists of up to 16 wt. % Al_2O_3, 6.9 wt. % Fe_2O_3, 4.1 wt. % K_2O, and 2.7 wt. % Na_2O, adjacent to steam separator HPS3. Scale metal concentration generally reduces with distance from the production well heads, although scale composition is quite variable in cross-section at each location; likely reflecting changes in geothermal brine chemistry/conditions. Micro chemical in-situ SEM-EDS analyses indicate that Al, K., Na, Ca (and some Fe) are in fact contained within the molecular structure of the silica itself, and are not merely present as crystalline aluminosilicate phases mixed with pure amorphous silica. Freshly deposited silica spheroids at the top of the scale samples were found to also be enriched with Al, K, Na, and Ca, indicating that alkali element uptake is rapid, and likely occurs during initial formation and growth Al-rich silica colloids. The scale appears to be an admixture of primary metal-rich colloids and later deposited pure SiO_2, which appears to plate onto the earlier deposited metal-rich colloids, and gradually in-fill void spaces within the metal-rich silica scale matrix. Preserved scale growth textures indicate that the scale, for the most part, grows via colloid impact and accumulation on the sharp leading edges of flow-perpendicular blades and ridges. This largely rules out conductive cooling of stationary brine during pipeline shut-down events as a significant source of pipeline scale accumulation. Scale XRD patterns are dominated by broad XRD peaks typical of amorphous opaline silica, though these record a systematic, compositionally dependent shift as the aluminium content in the scale varies; with greater Al concentrations correlating with larger 2Θ angles (Fig. 3). The single broad peaks of the XRD patterns, together with the compositional dependence of the peak positions, indicates that the scale is almost exclusively composed of amorphous material, with aluminium substituting into the silica structure, corroborating the SEM-EDS analyses. Together, these observations indicate that aluminium reacts with silica at the very earliest stages of silica scaling process.

To date, a plausible reaction mechanism has yet to be suggested which can account for the often rapid deposition of aluminium-rich silica scales from solutions frequently undersaturated with respect to amorphous silica, such as observed both at San Jacinto-Tizate in the SJ1-1 brine injection well head, and decommissioned SJ6-1 reinjection line (Thermochem, 2010), and several other geothermal fields internationally (Gallup, 1998; Raymond et al., 2005). Numerous studies investigating aspects of the aqueous silica-aluminium system over a very wide range of conditions indicate that kinetic reactions between aqueous monomeric silica and solid aluminium hydroxide/ oxyhydroxide are favourable, and may cause the rapid

formation of Al-silica colloids from solutions under-saturated with respect to amorphous silica (e.g. Exley and Birchall, 1993; Doucet et al. 2001a; Exley et al., 2002; Tokoro et al. 2014; Leiviska et al., 2014; Beardmore et al., 2016). Conversely, surface/adsorption reactions of polymerised silica with both $Al(OH)_{3(s)}$ and Al ions under the same conditions have not been observed (Bai et al. 2012), and been determined to kinetically unfavourable (Leiviska et al., 2014). The reaction mechanism proposed by Exley and Birchall (1993) to explain the formation hydroxy-aluminosilicates (HAS) may finally also provide the key to understanding and predicting the formation of geothermal aluminium-rich silica scales. This mechanism is triggered by the supersaturation of Al with respect to aluminium hydroxide, which may plausibly occur in many geothermal production wells and feed zones, though this has yet to be demonstrated.

6. FUTURE WORK

Work is currently underway investigating the possibility of a HAS type reaction of silica with aluminium at conditions more relevant to typical geothermal fluids via temperature and pH controlled laboratory experiments. A technique which may able to detect fluid-borne HAS-like species in geothermal brine is also being investigated.

ACKNOWLEDGEMENTS

The author would like to thank Polaris Infrastructure Ltd for permission to publish this paper, in particular J.V. Lawless for his invaluable support with this project, and J A Guidos of Polaris Energy S.A for his assistance with providing San Jacinto-Tizate plant technical details, and in collecting the scale samples. Also, the team of geoscientists and engineers at Jacobs New Zealand, in particular B.G. Lovelock; who freely shared their knowledge as well as technical, geological, and geochemical data concerning the San Jacinto-Tizate geothermal energy project. I would also like to thank S.J. Zarrouk, K.L Brown, and J.V. Rowland for providing much advice and many valuable comments.

REFERENCES

Arnórsson, S., 1995.: Geothermal systems in Iceland: structure and conceptual models—I. High-temperature areas. *Geothermics*, 24 (5-6), pp. 561-602.

Bai, S., Naren, G., Noma, H., Etou, M., Ohashi, H., Fujino, Y., Doi, K., Okaue, Y. and Yokoyama, T., 2012.: Silica deposition induced by isolated aluminum ions bound on chelate resin as a model compound of the surface of microbes. Colloids and Surfaces B: *Biointerfaces*, 95, pp. 208-213.

Beardmore, J., Lopez, X., Mujika, J.I. and Exley, C., 2016.: What is the mechanism of formation of hydroxyaluminosilicates? *Scientific Reports*, 6, pp. 30913.

Bénezeth, P., Palmer, D.A. and Wesolowski, D.J., 2001.: Aqueous high-temperature solubility studies. II. The solubility of boehmite at 0.03 m ionic strength as a function of temperature and pH as determined by in situ measurements. *Geochimica et Cosmochimica Acta*, 65(13), pp. 2097-2111.

Brigatti, M.F., Galan, E. and Theng, B.K.G., 2013.: Structure and mineralogy of clay minerals. *Developments in clay science*, 5, pp. 21-81.

Childs, C.W., Parfitt, R.L. and Newman, R.H., 1990.: Structural studies of Silica Springs allophane. *Clay Minerals*, 25(3), pp. 329-341.

Clemente, W.C. and villadolid-abrigo, F.L., 1993.: The Bulalo geothermal field, Philippines: reservoir characteristics and response to production. *Geothermics*, 22(5-6), pp. 381-394.

Doucet, F.J., Rotov, M.E. and Exley, C., 2001a.: Direct and indirect identification of the formation of hydroxyaluminosilicates in acidic solutions. *Journal of Inorganic Biochemistry*, 87(1), pp. 71-79.

Doucet, F.J., Schneider, C., Bones, S.J., Kretchmer, A., Moss, I., Tekely, P. and Exley, C., 2001b.: The formation of hydroxyaluminosilicates of geochemical and biological significance. *Geochimica Et Cosmochimica Acta*, 65(15), pp. 2461-2467.

Exley, C. and Birchall, J.D., 1993.: A mechanism of hydroxyaluminosilicate formation. *Polyhedron*, 12(9), pp. 1007-1017.

Exley, C., 2012.: Reflections upon and recent insight into the mechanism of formation of hydroxy-aluminosilicates and the therapeutic potential of silicic acid. *Coordination Chemistry Reviews*, 256(1-2), pp. 82-88.

Fleming, B.A. and Crerar, D.A., 1982.: Silicic acid ionization and calculation of silica solubility at elevated temperature and pH application to geothermal fluid processing and reinjection. *Geothermics*, 11(1), pp. 15-29.

Fujino, T. and Yamasaki, T., 1985.: Geologic and geothermal structure of the Hatchobaru field. *Geothermal Resources Council Bulletin*, pp. 11.

Gallup, D.L., 1997. Aluminum silicate scale formation and inhibition (1): scale characterization and laboratory experiments. *Geothermics*, 26(4) pp. 483-499.

Gallup, D.L., 1998.: Aluminum silicate scale formation and inhibition (2): scale solubilities and laboratory and field inhibition tests. *Geothermics*, 27(4) pp. 485-501.

Hickman, R.G., Dobson, P.F., Van Gerven, M., Sagala, B.D. and Gunderson, R.P., 2004.: Tectonic and stratigraphic evolution of the Sarulla graben geothermal area, North Sumatra, Indonesia. *Journal of Asian Earth Sciences*, 23(3) pp. 435-448.

Hiradate, S. and Wada, S.I., 2005.: Weathering process of volcanic glass to allophane determined by 27Al and 29Si solid-state NMR. *Clays and Clay Minerals*, 53(4), pp.401-408.

Ichikuni, M., 1970.: Incorporation of aluminum and iron into siliceous sinters. *Chemical Geology*, 6, pp. 273-279.

Itoi, R., Kumamoto, Y., Tanaka, T. and Takayama, J.:. History matching simulation of the Ogiri geothermal field, Japan. Proc. *World Geothermal Congress*, Bali, Indonesia. (2010).

Leiviska, T., Ramo, J., Lanzani, G., Huhtakangas, S., Laasonen, K. and Pehkonen, S.O., 2014.: Quasi-quantitative determination of elemental relationships and surface properties in aqueous aluminium-silicon systems. *Journal of Water Process Engineering*, 1, pp. 54-63.

Libbey, R., Lovelock, B., Ussher, G., 2017.: San Jacinto-Tizate draft conceptual model update, ZP00955-RPT-DR-045. *Jacobs New Zealand Limited*. Unpublished.

McNamara, D.D., Sewell, S., Buscarlet, E. and Wallis, I.C., 2016.: A review of the Rotokawa geothermal field, New Zealand. *Geothermics*, 59, pp. 281-293.

Mroczek, E.K., White, S.P. and Graham, D.J., 2000.: Deposition of amorphous silica in porous packed beds—predicting the lifetime of reinjection aquifers. *Geothermics*, 29(6), pp. 737-757.

Murakami, T., Kogure, T., Kadohara, H. and Ohnuki, T., 1998.: Formation of secondary minerals and its effect on anorthite dissolution. *American Mineralogist*, 83(12), pp. 1209-1219.

Palmer, D.A., D.J. Wesolowski, D.J., and Benezeth, P.: The aqueous chemistry of aluminum: A new approach to high temperature solubility measurements. *Proc. 21st Annual Workshop: Geothermal Reservoir Engineering*, Stanford, CA. (1996).

Portier, S., Vuataz, F.D., Barrios Martinez, A.L.: and Siddiqi, G.: Preliminary modelling of the permeability reduction in the injection zone at Berlin geothermal field, El Salvador, *Proc. World Geothermal Congress*, 22(2231) pp. 1-7. (2010).

Raymond, J., Williams-Jones, A.E. and Clark, J.R., 2005.: Mineralization associated with scale and altered rock and pipe fragments from the Berlin geothermal field, El Salvador; implications for metal transport in natural systems. *Journal of Volcanology and Geothermal Research*, 145(1-2), pp. 81-96.

Stimac, J., Nordquist, G., Suminar, A. and Sirad-Azwar, L., 2008.: An overview of the Awibengkok geothermal system, Indonesia. *Geothermics*, 37(3), pp. 300-331.

Strekopytov, S., Jarry, E. and Exley, C., 2006.: Further insight into the mechanism of formation of hydroxyaluminosilicates. *Polyhedron*, 25(17), pp.3399-3404.

Takenaka, T. and Furuya, S., 1991.: Geochemical model of the Takigami geothermal system, northeast Kyushu, Japan. *Geochemical Journal*, 25(4) pp. 267-281.

Thorhallsson, S., K. Ragnars, S. Arnórsson and H. Kristmannsdttir. Rapid scaling of silica in two district heating systems.: *2nd United Nations Symposium on the Development and Use of Geothermal Resources*, San Fransico, 1975.

Tokoro, C., Suzuki, S., Haraguchi, D. and Izawa, S., 2014.: Silicate removal in aluminum hydroxide co-precipitation process. *Materials*, 7(2) pp. 1084-1096.

Wesolowski, D.J. and Palmer, D.A., 1994.: Aluminum speciation and equilibria in aqueous solution: V. Gibbsite solubility at 50 C and pH 3–9 in 0.1 molal NaCl solutions (a general model for aluminum speciation; analytical methods). *Geochimica et Cosmochimica Acta*, 58(14), pp. 2947-2969.

Wells, N., Childs, C.W. and Downes, C.J., 1977.: Silica Springs, Tongariro National Park, New Zealand—analyses of the spring water and characterisation of the alumino-silicate deposit. *Geochimica et cosmochimica acta*, 41(10), pp. 1497-1506.

White, P., Lawless, J., Ussher, G. and Smith, A.: Recent results from the San Jacinto-Tizate geothermal field, Nicaragua. Proc. 30th *New Zealand Geothermal Workshop*, pp. 116-124. (2008).

Williams, L.A. and Crerar, D.A., 1985.: Silica diagenesis, II. General mechanisms. *Journal of Sedimentary Research*, 55(3), pp. 312-321.

Yokoyama, T., Y. Takahashi, T. Tarutani, R. Itoi and K. Jinno.: Behaviour of silicic acid and aluminium in geothermal water in the aging tank of Hatchobaru geothermal power station. *Proc. 8th NZ Geothermal Workshop*. (1987).

Yokoyama, T., Takahashi, Y., Yamanaka, C. and Tarutani, T., 1989.: Effect of aluminium on the polymerization silicic acid in aqueous solution and the deposition of silica of silica. *Geothermics*, 18(1-2), pp. 321-326.

Yokoyama, T., Sato, Y., Maeda, Y., Tarutani, T. and Itoi, R., 1993.: Siliceous deposits formed from geothermal water I. The major constituents and the existing states of iron and aluminium. *Geochemical Journal*, 27(6) pp. 375-384.

Zhu, C. and Lu, P., 2009.: Alkali feldspar dissolution and secondary mineral precipitation in batch systems: 3. Saturation states of product minerals and reaction paths. *Geochimica et Cosmochimica Acta*, 73(11), pp. 3171-3200.